The International Journal of Advanced Manufacturing Technology (2023) 126:1733–1746
https://doi.org/10.1007/s00170-023-11126-5

ORIGINAL ARTICLE

Development of low content Ti-x%wt. Mg alloys by mechanical milling plus hot isostatic pressing

Alex Humberto Restrepo Carvajal[1] · Jesús María Ríos[1] · Alejandro Alberto Zuleta[2] · Francisco Javier Bolívar[1] · Juan Guillermo Castaño[1] · Esteban Correa[3] · Félix Echeverria[1] · Mickaël Lambrecht[4] · María Isabel Lasanta[4] · Francisco Javier Pérez Trujillo[4]

Received: 24 October 2022 / Accepted: 15 February 2023 / Published online: 15 March 2023

Abstract
Several authors have shown promising results using Ti and Mg to develop materials that combine the benefits of these two metals, such as their low density and absence of harmful second phases, which makes them attractive for aerospace and biomedical applications as well as for hydrogen storage. However, titanium and magnesium are almost immiscible and there are great differences in processing temperatures of these two metals. Within the techniques reported in the literature for obtaining Ti-Mg alloys, powder metallurgy and high-energy ball milling are possibly the most popular. In this work, Ti and Mg powders were mixed using a high-energy ball mill and subsequently these mixes were sintered by hot isostatic pressing (HIP), under various conditions, to obtain Ti-Mg alloys with Mg %wt. close to the limit of solubility ($x < 2$%wt.). The results showed the influence of the sintering parameters in the microstructure of the sintered material, which allowed us to obtain a Ti-Mg alloy instead of a composite material.

Keywords Titanium-magnesium · Powder metallurgy · High-energy ball milling · Hot isostatic pressing

1 Introduction

Titanium and magnesium are used extensively in various industries due to their unique properties; it is for this reason that combining these two metals constitutes an important challenge for materials science [1–5]. Different results indicated that Ti-Mg materials could be attractive for hydrogen storage [6–8], aerospace [9, 10], and biomedical [11–14] among other applications. However, titanium and magnesium are almost immiscible and their melting points differ by around 1000 C [15]. Hence, maintaining molten titanium leads to substantial losses of magnesium by evaporation processes [16]. The phase diagram in Ti-Mg systems confirmed that under equilibrium conditions the miscibility of Mg in Ti is low [17]. The solubility of each metal into the other is less than 2 atomic % and intermetallic compounds are not found [18–21]. The valence of titanium is 4 while that of magnesium is only 2 [22, 23], Ti-Mg alloys have positive formation enthalpies [24, 25], and consequently, metallurgical alloying under thermodynamic equilibrium conditions is almost impossible.

In this sense, in the search to obtain Ti-Mg alloys, the use of processing techniques outside the thermodynamic equilibrium is one of the most likely methods [26]. Powder metallurgy and specially mechanical alloying (MA) is a process widely reported in studies seeking to manufacture Ti_x-Mg_{100-x} alloys with non-equilibrium compositions [27–30], which combined with thermal processes is the most appropriate way to achieve bulk alloys. The powders produced by mechanical alloying are first green compacted

✉ Alex Humberto Restrepo Carvajal
humberto.restrepo@udea.edu.co

[1] Centro de Investigación, Innovación y Desarrollo de Materiales – CIDEMAT, Facultad de Ingeniería, Universidad de Antioquia UdeA, Calle 70 No 52 – 21, Medellín, Colombia

[2] Grupo de Investigación de Estudios en Diseño - GED, Facultad de Diseño Industrial, Universidad Pontificia Bolivariana UPB, Circular 1 No 70 – 01, Medellín, Colombia

[3] Grupo de Investigación Materiales con Impacto – MAT&MPAC, Facultad de Ingenierías, Universidad de Medellín UdeM, Carrera 87 No 30 – 65, Medellín, Colombia

[4] Grupo de Investigación de Ingeniería de Superficies y Materiales Nanoestructurados, Facultad de Ciencias Químicas, Universidad Complutense de Madrid, Madrid, Spain

and thereafter sintered with a combination of temperature and time [15]. But the main drawback of this methodology is that high temperatures are required during the conventional sintering stage, affecting the stability of Ti_x-Mg_{100-x} alloys due to their metastable nature and low decomposition temperatures [31–33]. In this way, advanced technologies like hot isostatic pressing (HIP) have been implemented to allow bulk consolidation of these materials [16, 34–36].

In this work, an alternative process for consolidation of Ti-x%wt. Mg ($x < 2\%$) materials by means of HEBM and HIP is proposed. For this, one or two milling stages of HEBM and two HIP temperature conditions were studied in search of obtaining solubility of Mg into Ti after HIP. Finally, a characteristic microstructure in the titanium matrix was obtained, indicating the formation of an alloy instead of a composite material. Mechanical tests showed that the developed process increased some mechanical properties and degrade others as compared to pure Ti.

2 Experimental

2.1 Materials and methods

Commercial powders of titanium grade 2 (Fe: 0.04%; O_2: 0.15%; C: 0.02%; N: 0.02%; H_2: 0.001%; other: < 0.4% mass/mass; Ti: Bal.) and magnesium (99.81% purity) were milled in a Retsch *E*max high-energy ball mill, using zirconia balls in a 50-ml stainless steel vessel with zirconia coating and filled with n-hexane (process control agent-PCA). The milling container was operated in a globe box under high purity argon (Ar) atmosphere (H_2O and $O_2 < 1$ ppm) to avoid oxidation of the powders. In Table 1, the processing conditions of the two sort of samples studied here are presented, namely samples 1S and 2S. Sample 1S was obtained by only applying the mixing stage to the Mg and Ti as-received powders. For sample 2S, first the Ti and Mg powders were milled separately at different process conditions as described in Table 1, stage 1. After that, these milled powders were mixed in the *E*max (stage 2), under dry conditions using stearic acid (SA-2%wt.) as PCA.

The powders after processing in the HEBM were uniaxially compacted under a pressure of 1000 MPa for 15 min to obtain green samples with dimensions of 10 × 5 × 5 mm. Magnesium stearate was used as die lubricant. Then, the compacted samples were sintered by HIP under a UHP Ar atmosphere at 800 °C and 1050 °C, applying a pressure of 193 MPa for 1 h and 2 h respectively. The pressure was hold during the entire thermal cycle. The samples were preheated at 200° C for 1 h in the HIP in order to evaporate any remaining lubricant. Figure 1 presents the complete sample process.

2.2 Chemical, metallographic, and microstructural characterization

The chemical composition of all samples was performed by X-ray fluorescence according to ASTM E-539 using an Axios-PANalytical, and some samples were confirmed by ICP-OES.

The metallurgical structure was first analyzed in an Optical Microscope Nikon Eclipse 200. Previously all samples were polished using SiC papers from 180 to 1200 grits, and further prepared as mirror polish. All samples were etched with Kroll's reagent. At high magnification, the morphology of the sintered samples was analyzed using a scanning electron microscope (SEM) JEOL JSM-6490LV equipped with energy-dispersive X-ray (EDX) OXFORD INCAPentaFET-x3.

2.3 X-ray diffraction and TEM

The microstructural study and phase analysis was assessed by means of X-ray diffraction (Empyream Malvern-PANallytical), using CuKα radiation and scanning in the range $2\Theta = 20–90°$ with a step of 0.01°. The XRD peaks were analyzed by using the X'pert High Score Analysis software and JCPDS database (3.0e, PANalytical, Almelo, The Netherlands).

For TEM analysis, a thin film of the alloy was prepared by diamond wire cutting, abrading with fine-grit sandpaper, and final processing in a Gatan precision ion polishing (PIPS). Analysis in both STEM and TEM modes used a JEM-3000F equipment.

2.4 Microhardness tests

The mechanical behavior of sintered samples was determined by Vickers hardness tests. The VHT were performed according with the ASTM E18-18a standard. Vickers hardness measurements were carried out using a

Table 1 Condition of Ti–Cp and Mg milled powder

Sample code	Stage	Speed (rpm)	Time (h)	BPR	Ball size (mm)
1S	Mixing	600	10	8:1	10
2S	Stage 1 HEBM	Ti-1400 Mg-(1000/1400)	2 9	4.6:1 8:1/10:1	3 10/3
	Stage 2 mixing	600	10	8:1	10

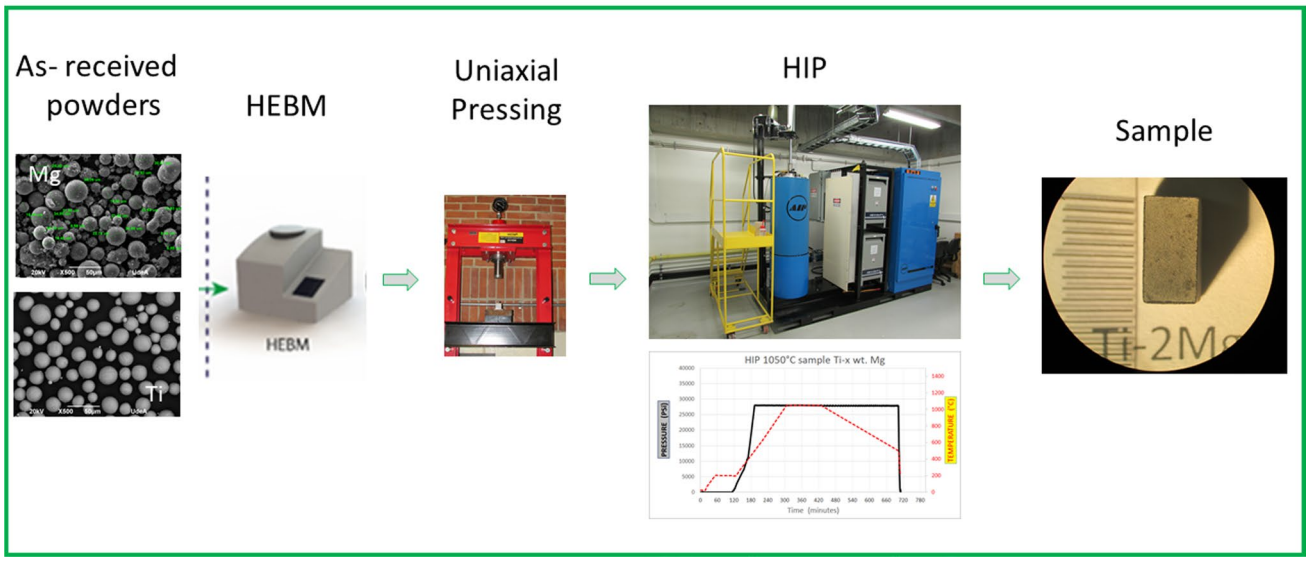

Fig. 1 Process to obtain Ti-Mg alloys with low alloy contain

Shimadzu Micro Vickers HMV-G21 hardness tester under a load of 1 kg with a dwell time of 15 s. Five measurements were made for each sample and the average value is reported in the results.

3 Results

3.1 Average composition of samples and microstructure

According to standard specification for "Powder Metallurgy (PM) Titanium and Titanium Alloy Structural Components" ASTM B988 [37], the use of X-ray fluorescence spectrometry is accepted as semi quantitative chemical analysis [38]. Some samples were examined by inductively coupled plasma optical emission spectroscopy (ICP-OES) to verify the XRF results. The chemical compositions for all processing conditions are shown in Fig. 2.

Although the amounts of Mg obtained are not exactly consistent with the amount of Mg added to the mixtures, it is clear for the samples sintered at high temperature (1050 °C) that the amount of Mg incorporated in the alloy is much lower than for the samples sintered at 800 °C, which implies a loss of magnesium in the process at high temperature due to volatilization of Mg [39]. At high temperature, the amount of Mg incorporated in samples 2S (two-step) is greater than for samples 1S, except for the sample Ti-2%wt. Mg (1S) HIP1050°C.

The results for the HIP treatment at 800 °C reveal a clear trend of progressive increase in the amount of Mg incorporated into the alloy, approaching to the expected composition in the mixtures. In a similar way for samples 2S, the amount of Mg incorporated in the alloy is higher compared to 1S, which means that in most cases, the two-step milling process incorporates more magnesium into the titanium.

Figure 3 shows four typical microstructures of samples sintered at 1050 °C in HIP. The images correspond to alloys with low alloy content (0.5% wt.) and high alloy content (2% wt.) of Mg. For the first condition, microstructure of fine and coarse lamellar morphology of α-Ti due to severe plastic deformation in the ball milling process is clear [40], which is consistent with the lower %wt. Mg (Fig. 3a). The second characteristic microstructure is equiaxed α-Ti plus a transformed beta Ti phase (lamellar phase), which corresponds to the samples with the greatest amount of magnesium (Fig. 3b). The dark zone corresponds to this second α/β colony phase. The third typical structure corresponds to a homogenous fine-grained structure Ti-α (Fig. 3c), and the last one is coarse equiaxed alpha plus the second dual-phase α/β (Fig. 3d).

Figure 4 shows four typical microstructures of the samples sintered at 800 °C in HIP. The images correspond to alloys with medium and high alloy content of Mg. At these conditions, a microstructure of fine α-Ti plus an acicular phase (from original particle) with a slightly elongated shape is clear. It can be seen that the greater the amount of this second phase, the greater the amount of magnesium

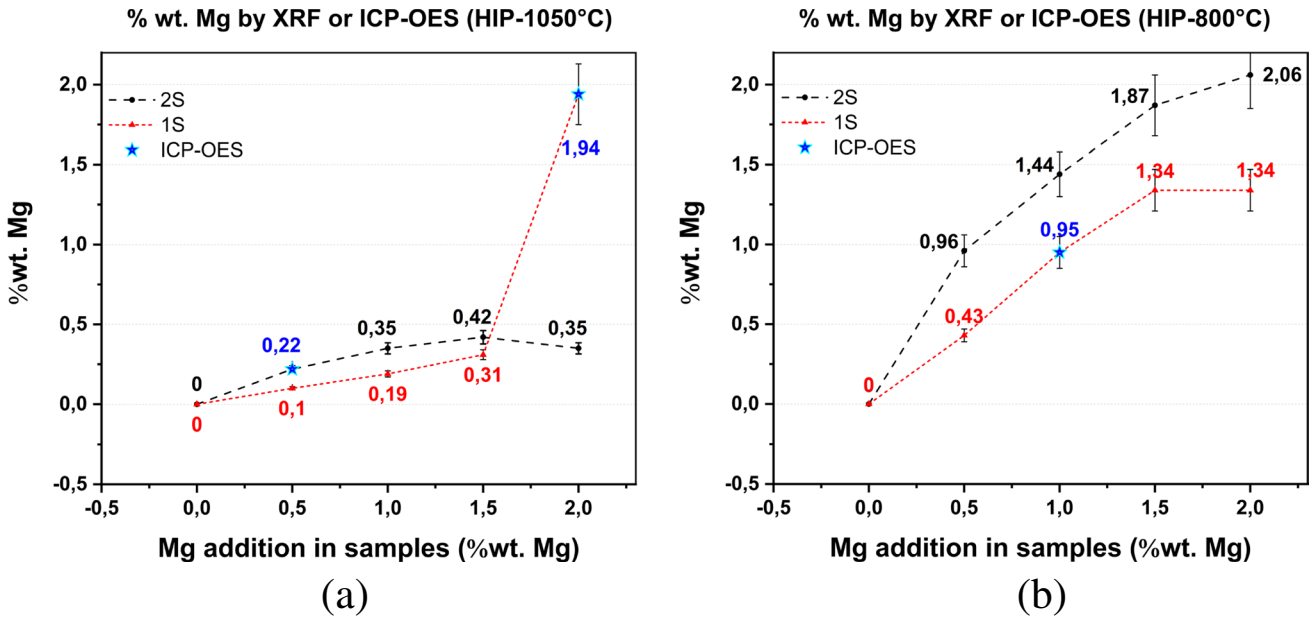

Fig. 2 Magnesium percentage in the alloys determined by XRF or ICP-OES. **a** HIP-1050 °C, two-step condition 2S (black) and one-step condition 1S (red). **b** HIP-800 °C, two-step condition 2S (black) and one-step condition 1S (red)

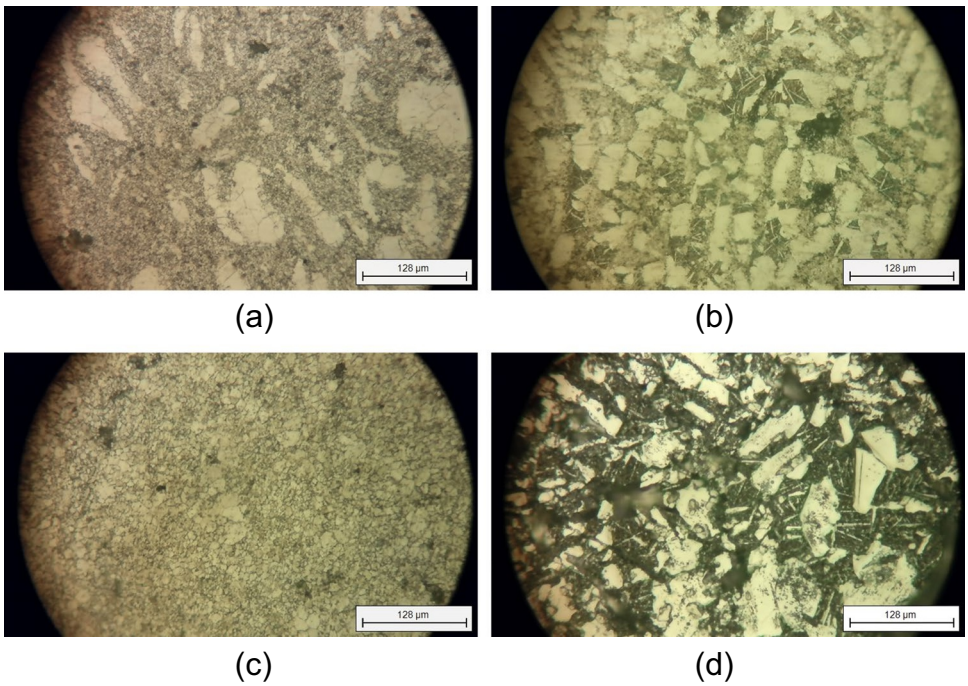

Fig. 3 Samples of Ti-x%wt. Mg sintered at 1050 °C in HIP at two different milling conditions. **a** Ti-0,5%wt. Mg (2S)-HIP 1050°C, **b** Ti-2%wt. Mg(2S)-HIP1050°C, **c** Ti-0,5%wt. Mg (1S)-HIP1050°C and **d** Ti-2%wt. Mg(1S)-HIP1050°C

incorporated in the sample according to the compositional analysis (Fig. 4b and d). At these conditions, some voids were present in the sample. These cavities are related to the chemical attack on the surface and discontinuities in the matrix due to its lower sintering temperature. Temperatures below 1000 °C for titanium sintering inevitably result in a loosely bonded Ti matrix [41].

To confirm the presence of magnesium in the second phase, SEM–EDS analysis was done in selected samples sintered at 1050 °C in HIP. The images in Fig. 5a show a microstructure typically transformed beta (alpha plus beta Ti), with some equiaxed grains inside it and basket-wave microstructure in the sintered samples [42]. The EDS analysis in this zone presented a broad Mg peak.

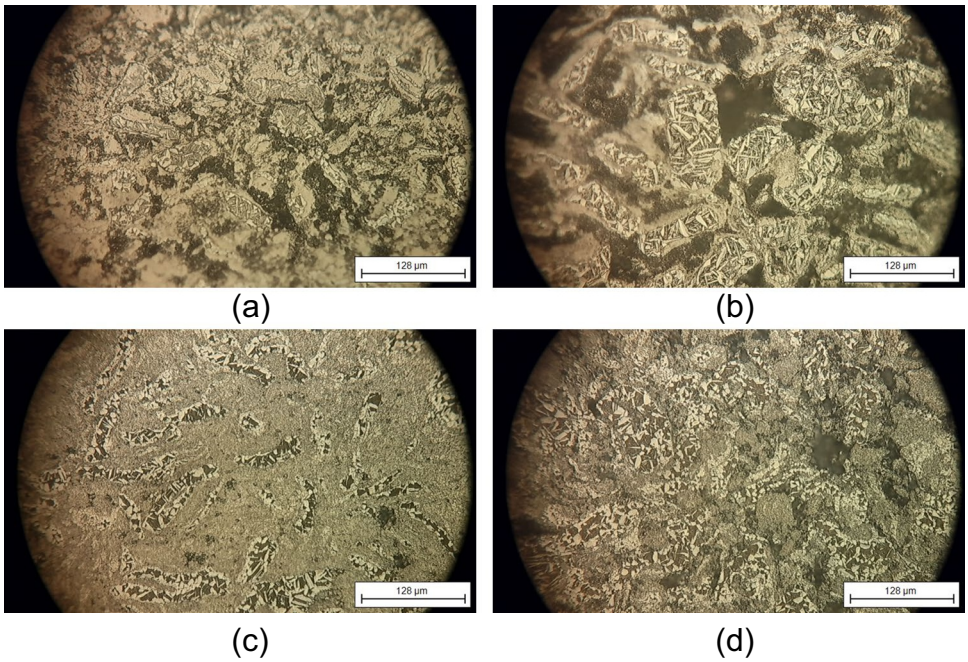

Fig. 4 Samples of Ti-x%wt. Mg sintered at 800 °C in HIP at two different milling conditions. **a** Ti-1%wt. Mg(2S)-HIP 800°C, **b** Ti-2%wt. Mg (2S)-HIP 800°C, **c** Ti-1%wt. Mg(1S)-HIP 800°C and **d** Ti-2%wt. Mg(1S)-HIP800°C

In contrast, the alloy showing a preferably equiaxed grain structure, which corresponds to the low Mg added (0.1% wt. Mg by XRF), did not show this Mg peak by EDS analysis; however, it is important to note that the concentration of the alloying element is within the detection limit of the technique of 0.1% [43] (Fig. 5b).

A similar trend is observed in the samples sintered at 800 °C in the HIP (Fig. 6); but in such a case, all samples contained a limited amount of this second dual phase. It is clear from the EDS analysis of the samples processed at 800 °C that the Mg peak heights agree with the amount of Mg added, where the highest peak represents a content of 2.06% wt. Mg, while the lowest peak represents a content of 1.03% wt. Mg (Fig. 6a and b).

According to our metallographic and SEM analysis of the samples sintered at both temperatures, this second dual phase is directly related to the amount of magnesium incorporated into the Ti matrix. From these images, it is not possible to observe any Mg particle isolated in the Ti matrix, as readily found in composite materials. Of course, we know that the titanium etching reagent leaches Mg particles that could be on the surface, but in the mirror polished samples sintered at high temperature (without etching), the two typical phases observed in composite materials (matrix and reinforcement) were not evident. The XRF analysis confirmed the presence of magnesium in the samples, so we can affirm that we obtained Ti-x%wt. Mg materials, whose amount of Mg depends on the manufacturing conditions.

3.2 XRD analysis

Figure 7 shows the XRD patterns of the different samples sintered at both temperatures and the phase identification.

At HIP-1050 °C for one-step (1S) or two-step (2S) samples, three phases were distinguishable, namely, Ti-α, TiC, and Ti-β, the latter being present with a low intensity only in the Ti-0.5%wt Mg (1S)-HIP1050°C sample. It can be observed from the peak height that for the samples with a two-step milling process, the amount of TiC is higher than for the one-step samples. The peaks corresponding to Mg are not visible even though Mg was found by XRF, which means that the element is in solution or its volume fraction was below the detection limit of X-ray diffraction.

At HIP-800 °C, the Ti-α, Mg, and Ti oxide compounds can be observed. At this temperature for the one-step samples, the intensity of the peaks of Ti oxides increased as the percentage of Mg decreases. These compounds may be associated with the thin oxide layer present in the as-received powders [41] and with chemical reactions with oxygen trapped in the pores remaining after compaction process, which did not close during HIP due to the low sintering temperature [44]. It is interesting to note a peak at $2\Theta = 50.5°$, which was not observed in the high-temperature samples and did not coincide with the crystalline planes of any of the phases analyzed. However, from the peak position, this signal may be associated with magnesium hydroxide present on the surface derived from a reaction with the humidity of the environment given the high reactivity of Mg and its higher content in the samples at HIP-800 °C [13].

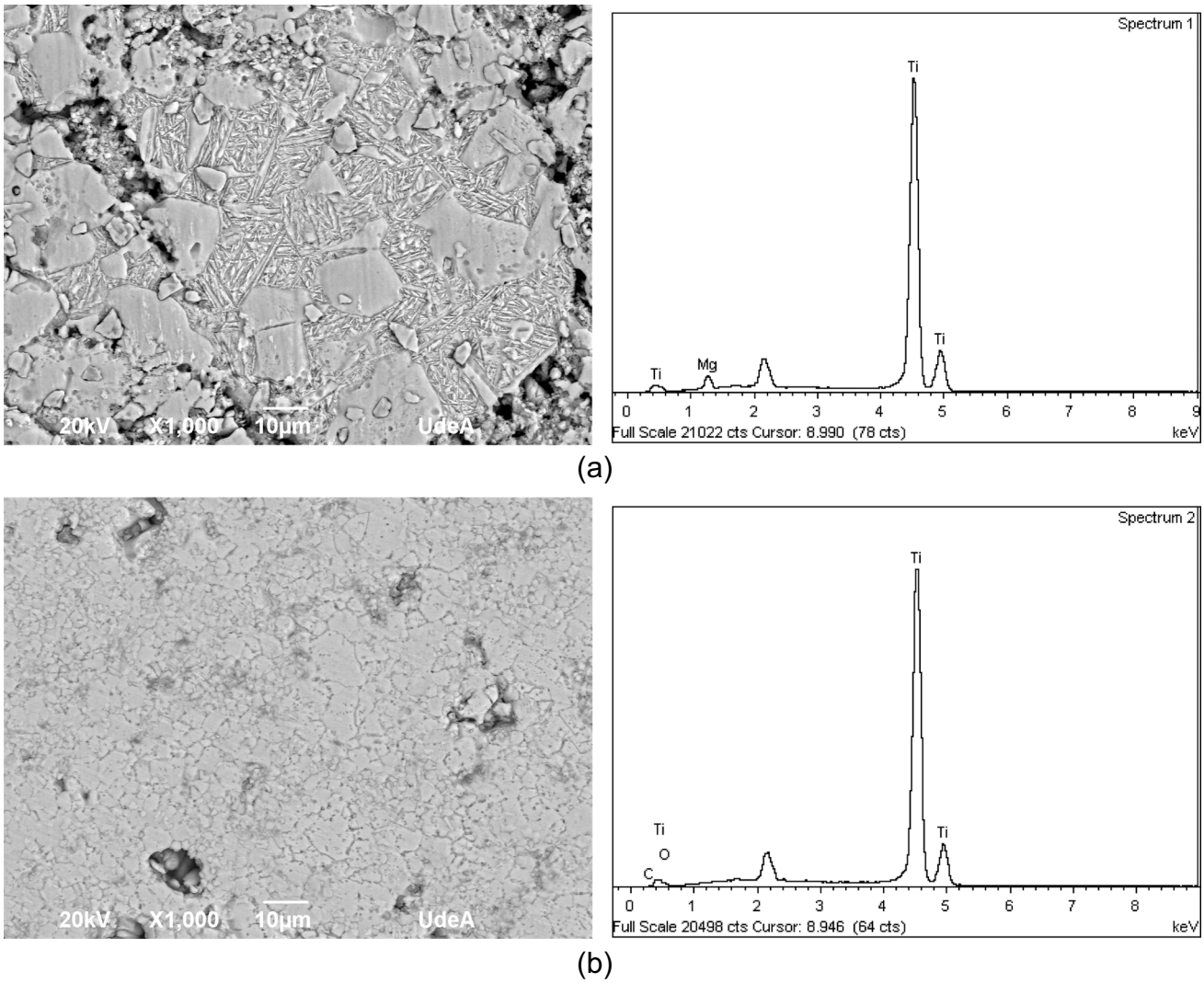

Fig. 5 SEM and EDS images of samples sintered at 1050 °C in HIP. **a** Ti-2%wt. Mg (1S). **b** Ti-0.5% wt. Mg (1S)

3.3 TEM analysis

To detect the presence of Mg inside the material, two selected samples were analyzed by TEM. Figure 8 shows a high-temperature sintering sample, and Fig. 9 the low-temperature sintered sample. The HAADF of Ti-2%wt. Mg (1S) HIP1050°C showed clusters of nanometric Mg grain which formed a magnesium-rich region close to grain boundaries and inside Ti grains [45]. Some magnesium oxide crystals could be seen too, but Mg is not uniformly distributed in the sample. In some areas and samples processed at the same HIP condition, it was difficult to identify its presence by TEM, which may indicate that it was selectively located at certain phases. The HAADF image also indicated that Mg was not always deposited at the grain boundaries (Fig. 8).

For the samples processed at low temperatures (Ti-2%wt. Mg (2S) HIP 800 °C), the STEM image showed a better distribution of Mg throughout the sample (Fig. 9a, b). Since Mg signals were detected by EDX throughout the matrix, it was clear that some Mg still exists as a solid solute in the titanium matrix [46]. Likewise, Mg nanoparticles can be observed in the Ti matrix as well as Ti and Mg crystals that form a coherent interface, which confirmed its iteration at an atomic scale (Fig. 9c).

3.4 Microhardness test

Figure 10 shows the Vickers micro hardness of Ti-x%wt. Mg alloys under different milling and HIP conditions. It was observed that the highest hardness values were

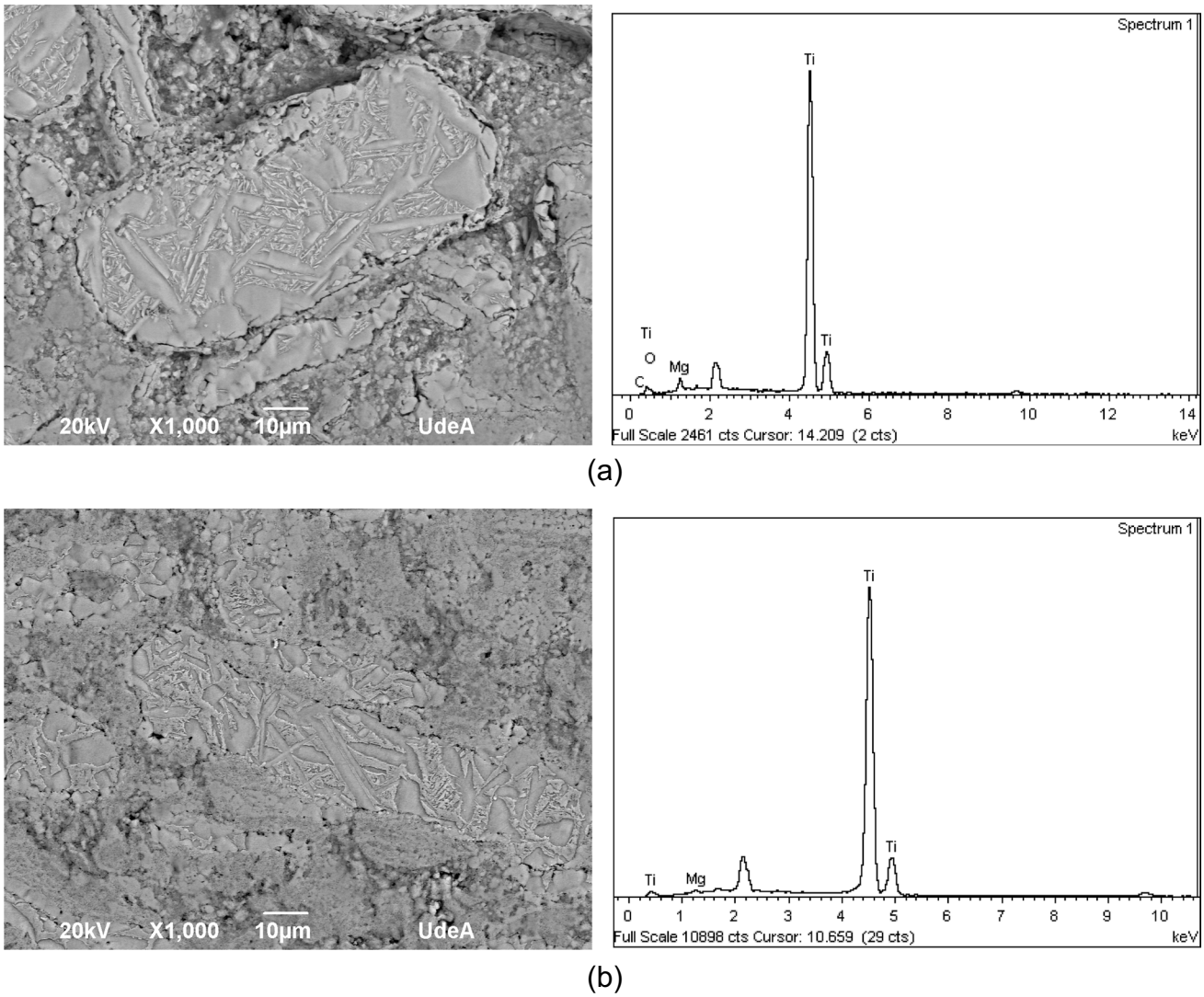

Fig. 6 SEM and EDS images of samples sintered at 800 °C in HIP. **a** Ti-2%wt. Mg (2S). **b** Ti-1% wt. Mg (1S)

obtained for samples sintered at 1050 °C compared to 800 °C for both milling conditions, 1S or 2S.

For the 2S samples (Fig. 10a.), the smaller particles help to improve melting, packing, and diffusion, improving the hardness of the material. Additionally, this powder, milled in liquid organic PCA, helped to promote the formation of hard phases, which increased the material hardness.

The graph does not show a trend in hardness concerning the percentage of magnesium added, but in any case, this property increases with the addition of Mg, compared with the pure Ti sample processed under the same conditions.

4 Discussion

In the reported binary phase diagram of the Ti-Mg system, the solubility of each metal into the other is less than 2 at.% [18, 20]. According to Murray [17] under equilibrium conditions, the solid solubility of magnesium in titanium is about 0.35% wt. at 890 °C and is as low as 0.10% wt. at 500 °C [23]. To enhance the solubility of Mg in Ti, non-equilibrium processing techniques can be utilized [47, 48]. Senkov et al. [19] reported a maximum solubility of Mg in α-Ti of 0.5%wt. and the solubility in β-Ti of 6%wt.

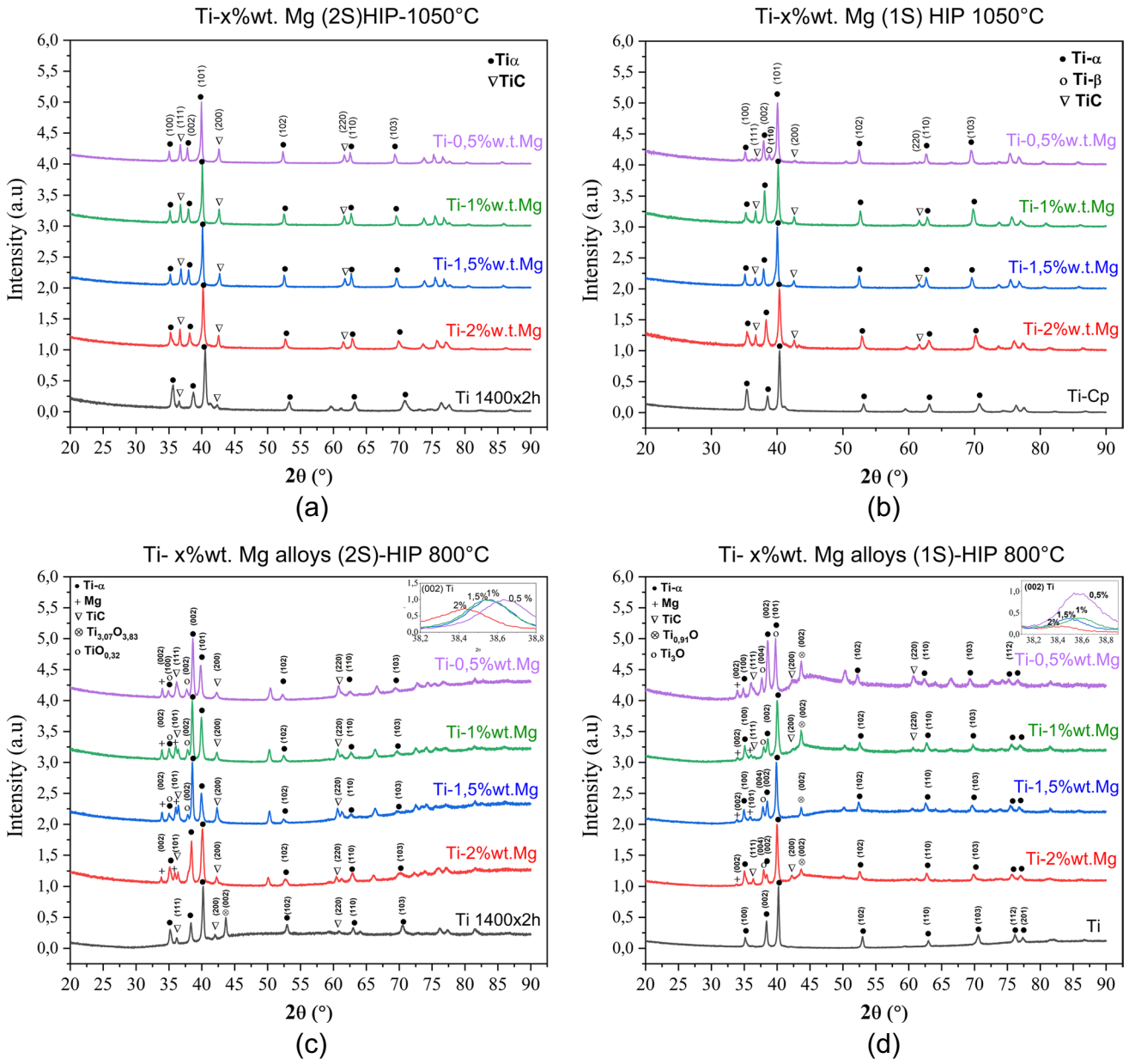

Fig. 7 XRD analysis of Ti-x%wt. Mg samples sintered at 1050 °C and 800 °C in HIP

This indicates that the increase in temperature or in the amount of beta-titanium phase enhances the solubility of Mg into Ti as discussed below. In the high-temperature HIP process, the amount of Mg is far less than at low temperature, but the XRD high-temperature pattern showed that no Mg phase was present, in spite of showing its presence by TEM and confirmed by ICP-OES. In this way, it is clear that the solubility of Mg in Ti sintered at high temperatures could be extended under certain processing conditions despite the phase diagram indicating a solubility less than 1%wt. [49]. These favorable conditions include the individual pregrinding process where the mechanical energy stored in the particles increases the free energy of the phases [23], and then the generation of more grain boundaries derived from comminution act as pathways to initiate solubilization [29], second for the generation of internal defects and dislocations, and finally for the high pressure and temperature conditions of the HIP which favor the sintering processes and also promote the diffusion of Ti and Mg atoms [41].

Few reports predict the interaction behavior of the alloying element Mg with Ti; however, some of them estimate that Mg is a beta phase stabilizer [17], and its effect is more noticeable at high temperatures [50]. Based on the quantity of

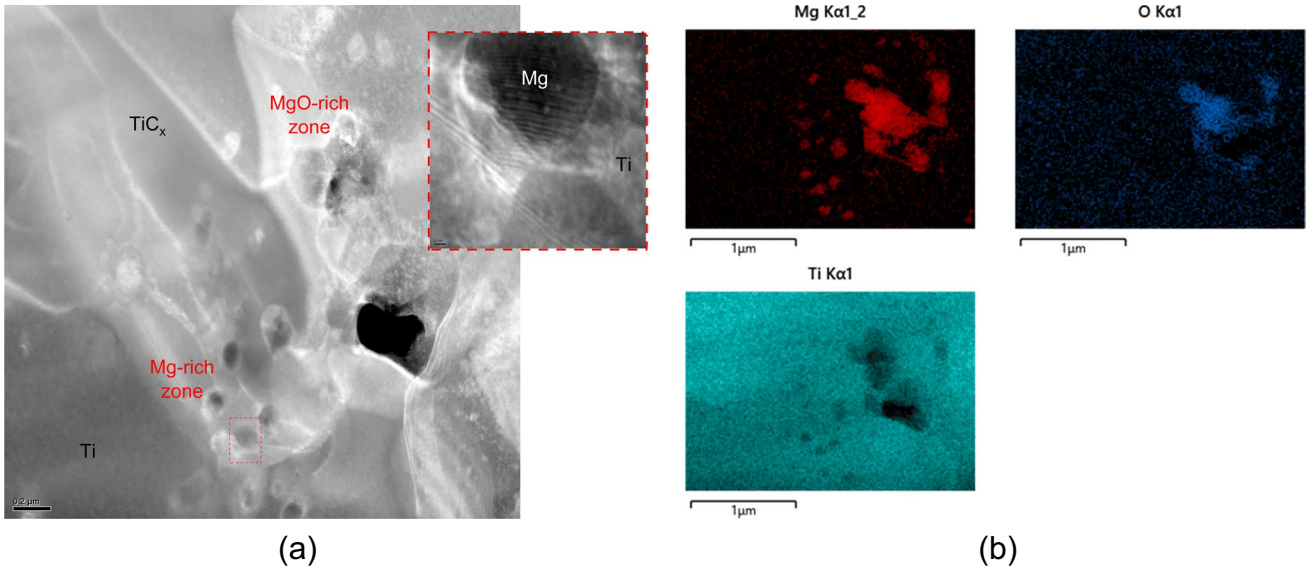

Fig. 8 High-temperature sample Ti-2%wt. Mg (1S)-HIP1050°C. **a** STEM-HAADF image Ti matrix and Mg nanograin. **b** Corresponding STEM-EDX mappings

alloying elements and phases present in the microstructures, small addition (1 to 2% wt.) of β stabilizer would lead to classifying the alloy as near alpha [51]. In practice, the near alpha alloys contain up to 2% wt. β stabilizing element which both introduce small amount of β-phase into the microstructure [52]. There is a relationship between the presence of the second phase in the microstructure and the amount of magnesium in our metal sample. When the amount of Mg was close to 0 (0.1% wt by XRF), the preferred microstructure was only equiaxial α-Ti, but when the amount of Mg was higher, the microstructure presented a bimodal microstructure typical of alpha plus beta alloys similar to that of Ti64 when cooled in air [53, 54].

At the high HIP sintering temperature (1050 °C), a higher amount of Mg may be lost due to the proximity to the Mg boiling point, but this temperature which is above the estimated β Transus (900 °C for this Ti–Cp by DSC) should allow a phase change of the powder after heating due to the HEBM processes and the incorporation of alloying elements. The presence of alpha phase might be developed due to alpha stabilizers like oxygen and carbon, and the presence of beta seems to be produced owing to Mg which is a beta stabilizer. This dual phase was found too in HDH Ti64-HIP980°C due to local overheating and outflowed beta stabilizing elements [55] as happens at high temperature in the HIP when approaching the vaporization temperature of magnesium. The thermal process plays an important role too. During the slow cooling in the HIP, the alpha phase nucleated at the beta grain boundary and the beta transformed into α + β phases as can be seen in the SEM images. The slow cooling rates of the sintering process in the HIP should reduce the nucleation rate of the α-phase. In the present case, the cooling rate used was 5 °C/min and the α/β clustering could be observed in the microstructure similar to other microstructures reported in Ti [42].

At low sintering temperature in the HIP (800 °C), the thermal process is more similar to the annealing heat treatment used for titanium alloys; a temperature below beta transus is reached and then the sample is cooled in the furnace. This can leave traces of cold or warm working in the microstructures of heavily worked samples and helps to obtain recrystallization. For commercial Ti–Cp and near-α alloys, the temperature of annealing treatment is close to 800 °C [54]. The final microstructure in our samples was incompletely recrystallized α, with a small volume fraction of dual-phase (α + β).

When studying the Ti-Mg system, it is clear from the XRD literature that a series of representative peaks exist in the 2Θ region 30–41°, corresponding to the (100), (002), and (101) planes of hexagonal Ti and Mg, or other crystal structures of both elements [25, 56, 57]. When comparing the XRD scans of Ti-wt.% Mg with different magnesium contents, a peak shift in this range appears. The systematic shift of the peaks from the magnesium towards the titanium position further indicates the formation of a single-phase solid solution and speculated successful alloying [11, 58]. Shifting in the peak position in the 2Θ ranges 35–35.5° and 37.8–38.4° agree with the supersaturating of Mg in Ti in HCP structures [47]. The above condition is fulfilled for both processing states at HIP-800 °C sintered powders (S1 and S2); however, at high temperature, the change is less noticeable than at low temperature, given the few quantities

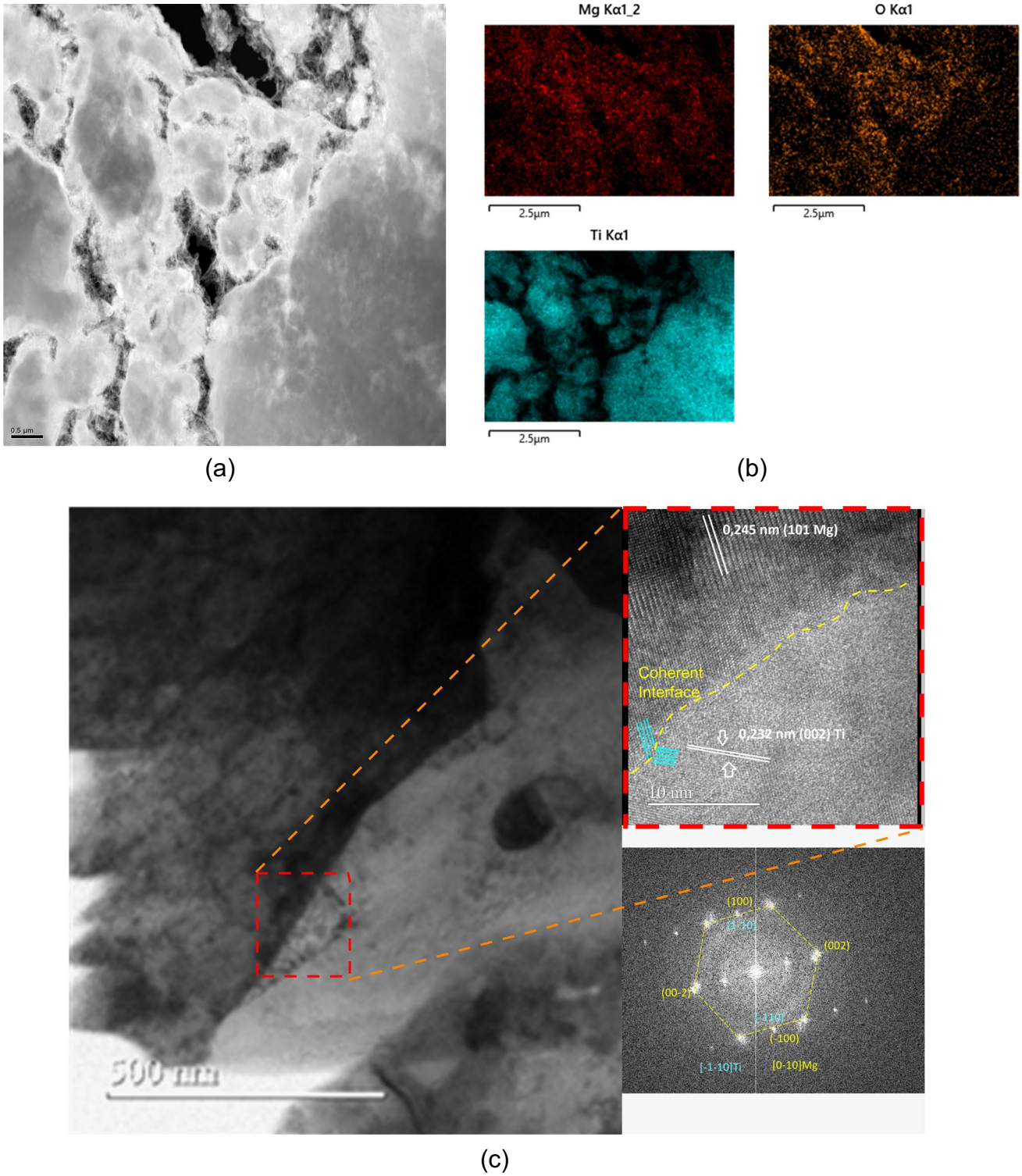

Fig. 9 Low-temperature sample Ti-2%wt. Mg (2S)-HIP800°C. **a** STEM-HAADF image Ti matrix and Mg. **b** Corresponding STEM-EDX mappings. **c** Coherent interface and SAED analysis

of Mg present in the alloys. At 800 °C HIP, the XRD of Ti-x%wt. Mg alloys shows a clear change in intensity and position in the peak of (002) plane of Ti-α. The shift to a lower diffraction angle is associated with the atomic radius of Mg which causes the expansion of the lattice parameter of the plane (002) [59]. The lattice volume expands due to

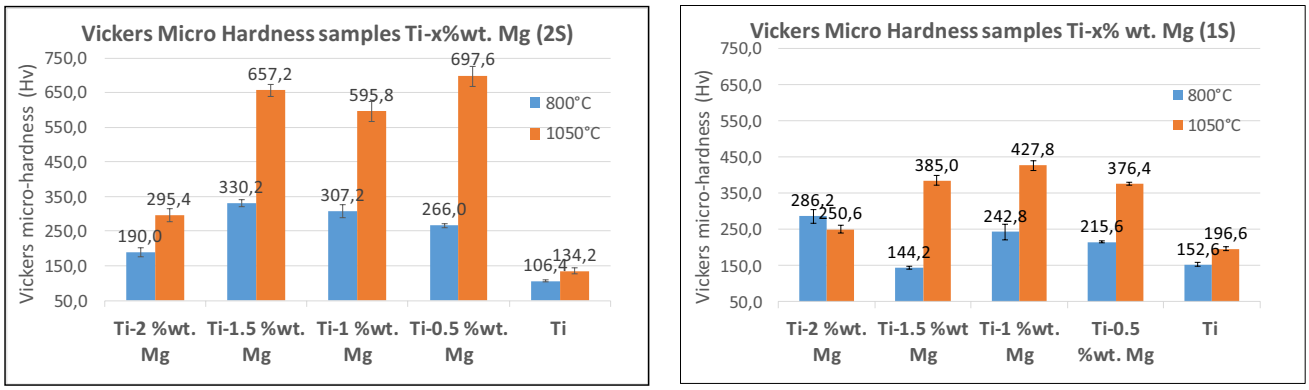

(a) Vickers micro hardness two step (2S) samples at HIP 1050°C and 800°C

(b) Vickers micro hardness one step (1S) sample at HIP 1050°C and 800°C

Fig. 10 Vickers micro hardness values of Ti-x%wt. Mg alloys under different process conditions

the accommodation of some Mg atoms in the Ti lattice [7]. When Mg contents do not significantly affect the position of Ti diffraction peaks, the alloying element (Mg) is not diffused [60] or its content is too low to be detected. At HIP-800 °C, a decrease in peak height and a progressive broadening of the (002) plane can be observed as the Mg content increases for both groups (1S and 2S—see insert), suggesting that the (002) plane texture in the samples is suppressed as more Mg atoms are mixed into Ti; additionally, it is also observed in the XRD that (100) and (101) textures are favored in our samples in a similar way to the reports for Ti-Mg alloys obtained by magnetron sputtering [58].

TEM images confirm the presence of Mg at the nanometric scale. It seems that it initially dissolves at the grain boundaries due to the number of crystals deposited there and then diffuses inwards [29]. Although the sintering temperature is high enough to evaporate part of the magnesium, the presence of these nanocrystalline Mg grains has been already reported in Ti alloys processed by HIP at high temperature and pressure [61] or by spark plasma sintering [39, 46]. The selected area diffraction pattern in the HIP 800 °C sample presented two close-packed hexagonal lattices related to Ti and Mg. Their orientation relationships can be expressed as (hkl) planes (100) Mg // (1–10) Ti (−100) Mg // (−110) Ti and correspond to one of the most likely matching crystalline planes with lesser interplanar spacing misfits [62]. This is a clear sign that a small amount of Ti existed in the Mg rich region or vice versa [39]. There are three types of phase boundary structures: coherent interface (form when the lattice misfits are $< \pm 10\%$), semi-coherent interfaces (lattice misfit of $< 20\%$), and incoherent interface (lattice misfits beyond 20%) [63]. According to cell parameter misfit of 9.76% and interplanar spacing misfit between (101) Mg // (002) Ti of less than 5.6%, a coherent interface forms between Mg and Ti matrix, which would lead to strong interfacial bonding in the alloys [4].

The correlation between Mg concentration and hardness of the Ti-Mg samples at low atomic concentration of Mg (< 0.2%wt.) was studied by Haruna et al. [64], finding a positive and almost linear relationship between the two parameters and reported a value of around 190 Hv for 0.1%wt. Mg. In the present work, the compositions evaluated were higher and although the hardness values obtained were in most cases above the values reported by Haruma et al., the existence of such a relationship with the Mg content is not clear. In the present study, the hardness of all samples initially increased with the increase in Mg content and then decreased when Mg was close to 2%wt. In the Ti-Mg samples with high alloying content produced by the Vapor Quenching route, the Vickers hardness of the deposit at 200 °C showed a similar tendency to our samples, reaching a maximum value of about 300 HV for about 4%wt of Mg and then decreased to 250 HV at 10% wt. [44]. In the present study, the hardness of the magnesium-bearing samples processed at high temperature was much higher than that of the samples processed at low temperature due to the presence of TiC phase and a better sintering temperature in the HIP for Ti alloys. At 800 °C, one possible cause for the lower hardness values could be an incomplete diffusion bonding across closed pores, which would be due to insufficient sintering temperature or processing time [1].

To better understand the potential magnesium inclusion into the titanium crystal structure, tracer diffusion coefficients of magnesium for temperatures up to 1200ºC were calculated with the ThermoCalc software, in a Ti98wt%-Mg2wt% system at atmospheric pressure, as seen in Fig. 11. It can be observed that for the 800ºC and 1050ºC working temperatures, magnesium atoms will diffuse preferentially into the bcc phase. The titanium allotropic temperature of compact-hexagonal (hcp) to bcc at 886ºC was not fully considered, as the bcc phase is supposed to coexist with hcp. In fact, it has been proposed that Mg

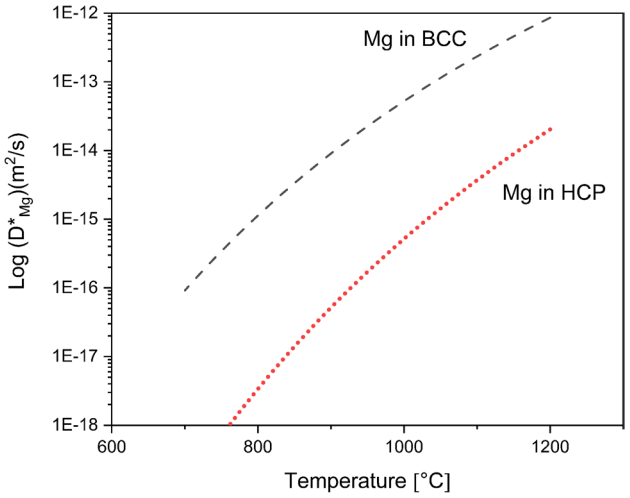

Fig. 11 Tracer diffusion coefficients of magnesium into compact hcp and bcc titanium, as function of temperature. ThermoCalc approach

addition can lead to a beta-stabilization during cooling [17] so magnesium inclusions into the titanium matrix could lead to a stabilization of beta-titanium at ambient temperature.

5 Conclusion

In this work, it was proved that it is possible to obtain Ti-Mg alloys with low quantities of Mg through high-energy ball milling coupled with hot isostatic pressing, offering a new process way for metastable alloy production. First, the amount of Mg introduced in the alloy was close to the reported limit of solubility. Then, titanium alloy microstructure and the atomic scale iteration between Ti and Mg allow us to assume that under the processing conditions described, the material was closer to an alloy than to a composite material. In addition, the quantity of Mg introduced into the alloys was directly related to the presence of the second binary $\alpha+\beta$ phase, depending on the processing parameters, mainly, the milling conditions and the sintering temperature in the HIP. Finally, the hardness was enhanced with the presence of TiC and (0.22–0.42)%wt. Mg in samples sintered at 1050 °C, leading to a 344% increase in hardness with respect to pure Ti.

Funding Open Access funding provided by Colombia Consortium The authors received funding from the Departamento Administrativo de Ciencia, Tecnología e Innovación–COLCIENCIAS (Project 111580862830, contract 183–2019), Universidad de Antioquia, Centro de Investigación para el Desarrollo y la Innovación (CIDI) of the Universidad Pontificia Bolivariana (Rad:482C-05/19–35) and Universidad de Medellín.

Data availability Not applicable.

Code availability Not applicable.

Declarations

Ethics approval Not applicable.

Consent to participate Not applicable.

Conflict of interest The authors declare no competing interests.

References

1. Fang ZZ, Paramore JD, Sun P, Ravi Chandran KS, Zhang Y, Xia Y, Cao F, Koopman M, Free M (2018) Powder metallurgy of titanium–past, present, and future. Int Mater Rev 63(7):407–459. https://doi.org/10.1080/09506608.2017.1366003
2. Esteban PG, Bolzoni L, Ruiz-Navas EM, Gordo E (2011) Introducción al procesado pulvimetalúrgico del titanio. Rev Metal 47(2):169–187. https://doi.org/10.3989/revmetalmadrid.0943
3. Bolokang AS, Phasha MJ, Motaung DE, Cummings FR, Muller TFG, Arend CJ (2014) Microstructure and phase transformation on milled and unmilled Ti induced by water quenching. Mater Lett 132:157–161. https://doi.org/10.1016/j.matlet.2014.06.063
4. Yu H, Sun Y, Hu L, Wan Z, Zhou H (2017) Microstructure and properties of mechanically milled AZ61 powders dispersed with submicron/nanometer Ti particulates. Mater Charact 127:272–278. https://doi.org/10.1016/J.MATCHAR.2017.03.017
5. Ouyang S, Huang Q, Liu Y, Ouyang Z, Liang L (2019) Powder metallurgical Ti-Mg metal-metal composites facilitate osteoconduction and osseointegration for orthopedic application. Bioact Mater 4:37–42. https://doi.org/10.1016/j.bioactmat.2018.12.001
6. Korablov D, Besenbacher F, Jensen TR (2014) Ternary compounds in the magnesium–titanium hydrogen storage system. Int J Hydrogen Energy 39:9700–9708. https://doi.org/10.1016/j.ijhydene.2014.03.141
7. Çakmak G, Károly Z, Mohai I, Ozturk T, Szepvolgyi J (2010) The processing of Mg–Ti for hydrogen storage; mechanical milling and plasma synthesis. Int J Hydrogen Energy 35:10412–10418. https://doi.org/10.1016/j.ijhydene.2010.08.013
8. Rousselot S, Bichat M-P, Guay D, Roué L (2019) Structure and electrochemical hydrogen storage properties of Mg-Ti based materials prepared by mechanical alloying. ECS Trans 16:91–100. https://doi.org/10.1149/1.3112733
9. Ye HZ, Liu XY (2005) Microstructure and tensile properties of Ti6Al4V/AM60B magnesium matrix composite. J Alloys Compd 402:162–169. https://doi.org/10.1016/j.jallcom.2005.04.175
10. Xianhua C, Yuxiao G, Fusheng P (2016) Research progress in magnesium alloys as functional materials. Rare Met Mater Eng 45(9):2269–2274. https://doi.org/10.1016/S1875-5372(17)30015-2

11. Hoffmann I, Cheng Y-T, Puleo DA, Song G, Waldo RA (2011) Mg-Ti: a possible biodegradable, biocompatible, mechanically matched material for temporary implants. MRS Proc 1301:mrsf10-1301-oo06-07. https://doi.org/10.1557/opl.2011.566
12. Liu Y, Li K, Luo T, Song M, Wu H, Xiao J, Tan Y, Cheng M, Chen B, Niu X, Hu R, Li X, Tang H (2015) Powder metallurgical low-modulus Ti-Mg alloys for biomedical applications. Mater Sci Eng C 56:241–250. https://doi.org/10.1016/j.msec.2015.06.010
13. Balog M, Ibrahim AMH, Krizik P, Klimova A, Catic A, Schauperl Z (2019) Bioactive Ti + Mg composites fabricated by powder metallurgy: the relation between the microstructure and mechanical properties. J Mech Behav Biomed Mater 90:45–53. https://doi.org/10.1016/j.jmbbm.2018.10.008
14. Cetin Y, Ibrahim AMH, Gungor A, Yildzhan Y, Balog M, Krizik P (2020) In-vitro evaluation of a partially biodegradable TiMg dental implant: the cytotoxicity, genotoxicity, and oxidative stress. Materialia 14:100899. https://doi.org/10.1016/j.mtla.2020.100899
15. Machio C, Nyabadza D, Sibanda V, Chikwanda HK (2011) Characterization of mechanically alloyed f.c.c. Ti–Mg-based powders. Powder Technol 207:387–395. https://doi.org/10.1016/j.powtec.2010.11.023
16. Suryanarayana C, Froes FH (1990) Nanocrystalline titanium-magnesium alloys through mechanical alloying. J Mater Res 5:1880–1886. https://doi.org/10.1557/JMR.1990.1880
17. Murray JL (1986) The Mg−Ti (magnesium-titanium) system. Bull Alloy Phase Diagrams 7:245–248. https://doi.org/10.1007/BF02868999
18. Asano K, Enoki H, Akiba E (2009) Synthesis of HCP, FCC and BCC structure alloys in the Mg-Ti binary system by means of ball milling. J Alloys Compd 480:558–563. https://doi.org/10.1016/j.jallcom.2009.01.086
19. Senkov O, Cavusoglu M, Froes FH Sam (2000) Synthesis of a low-density Ti–Mg–Si alloy. J Alloys Compd 297:246–252. https://doi.org/10.1016/S0925-8388(99)00558-7
20. Lu W-C, Ou S-F, Lin M-H, Wong M-F (2016) Hydriding characteristics of Mg–Ti alloys prepared by reactive mechanical grinding and hydrogen pulverization. J Alloys Compd 664:193–198. https://doi.org/10.1016/J.JALLCOM.2015.12.064
21. Wuquiang A, Yaojun L, Fei C (2022) Microstructure and mechanical properties of Ti–Mg lightweight heterostructured materials. Mater Sci Eng A 850:143560
22. Kalisvaart WP, Wondergem HJ, Bakker F, Notten PHL (2007) Mg–Ti based materials for electrochemical hydrogen storage. J Mater Res 22:1640–1649. https://doi.org/10.1557/JMR.2007.0195
23. Zhou E, Suryanarayana C, Froes FH, (Sam), (1995) Effect of pre-milling elemental powders on solid solubility extension of magnesium in titanium by mechanical alloying. Mater Lett 23:27–31. https://doi.org/10.1016/0167-577X(95)00009-7
24. Zhao J, Wen F, Feng K, Wang GuC, Y, (2022) Interface microstructure regulation of Mg/Ti bimetals by thermal diffusion treatment of Ni-coated TC4 alloy. Intermetallics 147:107594. https://doi.org/10.1016/j.intermet.2022.107594
25. Liang G, Schulz R (2003) Synthesis of Mg-Ti alloy by mechanical alloying. J Mater Sci 38:1179–1184. https://doi.org/10.1023/A:1022889100360
26. Asano K, Kim H, Sakaki K, Page K, Hayashi S, Nakamura Y, Akiba E (2014) Synthesis and structural study of Ti-rich Mg–Ti hydrides. J Alloys Compd 593:132–136. https://doi.org/10.1016/J.JALLCOM.2014.01.061
27. Rousselot S, Bichat MP, Guay D, Roué L (2008) Structure and electrochemical behaviour of metastable Mg50Ti50 alloy prepared by ball milling. J Power Sources 175:621–624. https://doi.org/10.1016/j.jpowsour.2007.09.022
28. Suryanarayana C (2001) Mechanical alloying and milling. Prog Mater Sci 46:1–184. https://doi.org/10.1016/S0079-6425(99)00010-9
29. Sun F, Sam FFH (2002) Synthesis and characterization of mechanical-alloyed Ti–xMg alloys. J Alloys Compd 340:220–225. https://doi.org/10.1016/S0925-8388(01)02027-8
30. Wei XS, Xu W, Xia K (2014) Metastable orthorhombic phases at ambient pressure in mechanically milled pure Ti and Ti–Mg. Scr Mater 93:32–35. https://doi.org/10.1016/j.scriptamat.2014.08.024
31. Hida M, Asai K, Takemoto Y, Sakakibara A (1997) Solid solubility in nanocrystalline Ti/Mg and Mg/Ti composites powder produced by mechanical alloying. Mater Sci Forum 235–238:187–192. https://doi.org/10.4028/www.scientific.net/MSF.235-238.187
32. Cai XC, Song J, Yang TT, Peng QM, Huang JY, Shen TD (2018) A bulk nanocrystalline Mg–Ti alloy with high thermal stability and strength. Mater Lett 210:121–123. https://doi.org/10.1016/j.matlet.2017.09.021
33. Cai XC, Sun BR, Liu Y, Zhang N, Zhang N, Zhang JH, Yu H, Huang JY, Peng QM, Shen TD (2018) Selection of grain-boundary segregation elements for achieving stable and strong nanocrystalline Mg. Mater Sci Eng A 717:144–153. https://doi.org/10.1016/j.msea.2018.01.058
34. Cai C, He S, Li L, Teng Q, Song B, Yan C, Wei Q, Shi Y (2019) In-situ TiB/Ti-6Al-4V composites with a tailored architecture produced by hot isostatic pressing: microstructure evolution, enhanced tensile properties and strengthening mechanisms. Compos B 164:546–558. https://doi.org/10.1016/j.compositesb.2019.01.080
35. Zhang K, Mei J, Wain N, Wu X (2010) Effect of hot-isostatic-pressing parameters on the microstructure and properties of powder Ti-6Al-4V hot-isostatically-pressed samples. Metallurgical and Materials Trans A 41A:1033–1045. https://doi.org/10.1007/s11661-009-0149-y
36. Hübler D, Ghasemi A, Riedel R, Fleck C, Kamrani S (2020) Effect of hot isostatic pressing on densification, microstructure and nanoindentation behaviour of Mg–SiC nanocomposites. J Mater Sci 55:10582–10592. https://doi.org/10.1007/s10853-020-04758-5
37. ASTM B988–18 (2018) Standard specification for powder metallurgy (PM) titanium and titanium alloy structural components
38. ASTM E539–19 (2019) Standard test method for analysis of titanium alloys by wavelength dispersive X-ray fluorescence spectrometry
39. Liang L, Huang Q, Wu H, Ouyang Z, Liu T, He H, Xia J, Lei G, Zhou K (2021) Stimulation of in vitro and in vivo osteogenesis by Ti-Mg composite materials with the sustained-release function of magnesium ions. Colloids Surfaces B Biointerfaces 197:111360. https://doi.org/10.1016/j.colsurfb.2020.111360
40. Long Y, Guo WJ, Li Y (2016) Bimodal-grained Ti fabricated by high-energy ball milling and spark plasma sintering. Trans Nonferrous Met Soc China (English Ed) 26:1170–1175. https://doi.org/10.1016/S1003-6326(16)64216-4
41. Cai X, Ding S, Li Z, Zhan X, Wen K, Xu l, Zhang Y, Peng Y, Shen T, (2021) Simultaneous sintering of low-melting-point Mg with high-melting-point Ti via a novel one-step high-pressure solid-phase sintering strategy. J Alloys Compd 858:158344. https://doi.org/10.1016/j.jallcom.2020.158344
42. Moghadam MS, Fayyaz A, Ardestani M (2021) Fabrication of titanium components by low-pressure powder injection moulding using hydride-dehydride titanium powder. Powder Technol 377:70–79. https://doi.org/10.1016/j.powtec.2020.08.075
43. Nasrazadani S, Hassani S (2016) Modern analytical techniques in failure analysis of aerospace, chemical, and oil and gas industries. Handbook of Materials Failure Analysis with Case Studies from the Oil and Gas Industry. 39–54

44. Ward-Close CM, Lu G, Partridge PG (1994) Microstructure of vapour-quenched Ti-Mg alloys. Mater Sci Eng A 189:247–255. https://doi.org/10.1016/0921-5093(94)90422-7
45. Bárcena-González G, Guerrero-Lebrero MP, Guerrero E, Yañez A, Nuñez-Moraleda B, Kepaptsoglou D, Lazarov VK, Galindo P (2019) HAADF-STEM image resolution enhancement using high-quality image reconstruction techniques: case of the Fe3O4(111) surface. Microsc Microanal 25:1297–1303. https://doi.org/10.1017/S1431927619014788
46. Liang L, Song D, Wu K, Ouyang Z, Huang Q, Lei G, Zhou K, Xiao J, Wu H (2022) Sequential activation of M1 and M2 phenotypes in macrophages by Mg degradation from Ti-Mg alloy for enhanced osteogenesis. Biomater Res 26:1–19. https://doi.org/10.1186/s40824-022-00262-w
47. Edalati K, Emami H, Staykov A, Smith AJ, Akiba E, Horita Z (2015) Formation of metastable phases in magnesium - titanium system by high-pressure torsion and their hydrogen storage performance. Acta Mater 99:150–156. https://doi.org/10.1016/j.actamat.2015.07.060
48. Zhen JG, Partridge PG, Steeds JW, Dm W, Ward-close CM (1997) Microstructure of vapour quenched Ti–29 wt% Mg alloy solid solution. J Mater Sci 32:3089–3099. https://doi.org/10.1023/A:1018682130018
49. Tejeda-Ochoa A, Kametani N, Carreño-Gallardo C, Ledezma-Sillas JE, Adachi N, Todaka Y, Herrera Ramirez JM (2020) Formation of a metastable fcc phase and high Mg solubility in the Ti-Mg system by mechanical alloying. Powder Technol 374:348–352. https://doi.org/10.1016/j.powtec.2020.07.053
50. Rossi MC, Bayerlein DL, Gouvêa EDS, Haro Rodríguez M, Escuder A, Borras V (2021) Evaluation of the influence of low Mg content on the mechanical and microstructural properties of β titanium alloy. J Mater Res Technol 10:916–925. https://doi.org/10.1016/j.jmrt.2020.12.103
51. VydehiArun J (2006) Titanium alloys: an atlas of structures and fracture features. Physical Metallurgy of Titanium Alloys. CRC Taylor and Francis, Boca Raton
52. Polmear IJ (2006) Light alloys. From traditional alloys to nanocrystals.Butterworth, 4th ed.
53. Kestler H, Clemens H, Leyens C, Peters M (2003) Titanium and titanium alloys
54. Donachie M (2000) TITANIUM, a Technical Guide,2nd ed ASM International
55. Kim Y, Kim EP, Song YB, Lee SH, Kwon YS (2014) Microstructure and mechanical properties of hot isostatically pressed Ti-6Al-4V alloy. J Alloys Compd 603:207–212. https://doi.org/10.1016/j.jallcom.2014.03.022
56. Hoffmann I (2014) Magnesium-titanium alloys for biomedical applications. University of Kentucky
57. Asano K, Enoki H, Akiba E (2009) Synthesis process of Mg–Ti BCC alloys by means of ball milling. J Alloys Compd 486:115–123. https://doi.org/10.1016/j.jallcom.2009.06.140
58. Song G-L, Haddad D (2011) The topography of magnetron sputter-deposited Mg–Ti alloy thin films. Mater Chem Phys 125:548–552. https://doi.org/10.1016/j.matchemphys.2010.10.018
59. Hieda J, Niinomi M, Nakai M, Cho K (2015) In vitro biocompatibility of Ti–Mg alloys fabricated by direct current magnetron sputtering. Mater Sci Eng C 54:1–7. https://doi.org/10.1016/j.msec.2015.04.029
60. Lai T, Xu JL, Huang J, Wang Q, Zhang JP, Luo JM (2022) Partially biodegradable Ti–Mg composites prepared by microwave sintering for biomedical application. Mater Charact 185:111748. https://doi.org/10.1016/j.matchar.2022.111748
61. Sun F-S, Froes FH Sam (2003) Effect of Mg on the microstructure and properties of TiAl alloys. Mater Sci Eng A 345:255–261. https://doi.org/10.1016/S0921-5093(02)00479-3
62. Yang H, Chen X, Huang G, Song J, She J, Tan J, Zheng K, Jin Y, Jiang B, Pan F (2022) Microstructures and mechanical properties of titanium-reinforced magnesium matrix composites: review and perspective. J Magnes Alloy 10:2311–2333. https://doi.org/10.1016/j.jma.2022.07.008
63. Bhattacharyya A, Maurice D (2018) On the evolution of stresses due to lattice misfit at a Ni-superalloy and YSZ interface. Surfaces and Interfaces 12:86–94. https://doi.org/10.1016/j.surfin.2018.05.007
64. Haruna T, Motoya D, Nakagawa Y, Oishi T (2013) Corrosion resistance of titanium-magnesium alloy in weak acid solution containing fluoride ions. Nippon Kinzoku Gakkaishi/Journal Japan Inst Met 77:328–333. https://doi.org/10.2320/jinstmet.J2013026